SAR Raw Signal Simulation for Urban Structures

Giorgio Franceschetti, *Life Fellow, IEEE*, Antonio Iodice, *Member, IEEE*, Daniele Riccio, *Senior Member, IEEE*, and Giuseppe Ruello, *Student Member, IEEE*

***Abstract*—In this paper, a synthetic aperture radar (SAR) raw signal simulator for urban scenes is presented along with models it employs to compute the backscattered field and to account for the imaging radar sensor characteristics. Urban areas are represented as a set of dielectric buildings placed over a random rough nonflat dielectric terrain. The adopted models allow evaluation of the raw signal on a sound physical and mathematical background: the scattering model employs the Kirchhoff approach appropriately extended to include multiple-reflection effects, and the radar model operates in the two-dimensional Fourier transformed domain. Details to assess how and why the simulator is also efficient with respect to the computational time are provided. In addition, relevant examples are discussed to show the simulator potentialities and assess the validity of the main results. It is shown that the simulator is able to quantitatively assess performances of SAR sensors over urban structures. The proposed simulator turns out to be also useful to train numerical schemes devoted to feature extraction, and to test any specific SAR processing technique. Comments for further developments of the simulation tool are presented.**

***Index Terms*—Buildings, radar scattering, synthetic aperture radar (SAR), urban areas, simulation.**

I. Introduction and Motivations

MODERN cities are continuously changing dynamical environments where most of the human activities take place. Hence, a frequently updated development check is extremely important in order to plan optimal resources distribution and to face population migrations [1]: these points are of paramount importance in developing countries. A continuous monitoring is required to support urban areas planning activities: to this aim, thematic maps and censuses are usually realized, even if they are often money and time consuming, obtained data are less accurate than needed, and they reach the decisional centers with a delay that is unacceptable for prompt responses. This is basically due to the inadequateness of available classical instruments.

It is now widely agreed that use of new remote sensing instruments might provide a huge amount of information and appropriate monitoring tools to collect cheap and timely data to be used in resources and land use management [1]. In addition, remote sensing instruments may provide information useful to disaster monitoring, for example quickly detecting the damages caused by an earthquake. Among remote sensing instruments, extremely interesting features are represented by synoptic view, and independence from weather conditions and solar illumination. It is well known that the remote sensor holding these fundamental properties is the synthetic aperture radar (SAR). However, the main obstacle to recognize the SAR sensors as a key tool for urban settlements monitoring is the acknowledged lack of electromagnetic and radar models that are able to quantitatively predict and explain SAR image relevant to urban scenes [2]; even for canonical scenes representing a single dielectric building and a flat dielectric background, quantitative studies that fully explain the link between building properties, sensor characteristics and the corresponding SAR image are currently not available. Then, SAR images of urban areas are continuously acquired by the available SAR sensors, but, in practise, users are not able to extract from those images useful information: so far, the main effort to apply SAR images to urban areas monitoring has been devoted to detection, exploiting the fact that the urban areas appear as brighter pixels in a SAR image; the huge complexity of the electromagnetic phenomena that occur in urban areas posed a severe limit to any further investigation [1], [2].

In order to fully exploit the SAR sensor characteristics and to optimize its design, the SAR raw signal simulation is a fundamental tool. First of all, it allows managing appropriate canonical scenes: in the SAR simulation (direct problem) the scene and sensor parameters are input data, and the SAR raw data and (if required) SAR images are computed. If the SAR simulator is developed on the basis of physical and mathematical models, it turns out to be crucial in the extraction of information on urban areas from SAR data. In fact, it allows to face the inverse problem again on physical bases. Moreover, an appropriately designed simulation tool can be able to also manage more realistic situations wherein several buildings with different characteristics are present on a nonflat terrain.

One further reason that has limited the study on SAR images of urban areas relies on the poor resolution that is actually obtained by available spaceborne sensors with respect to the information content to be monitored in an urban area. It is commonly believed that the low resolution of actually available sensors did not allow the extraction of much information. This assumption is no longer valid since the new generation of spaceborne SAR sensors is planned to achieve resolutions at the scale of 1 m. Accordingly, in view of the new generation of high-resolution SAR sensors, it would be highly desirable that an appropriate simulation tool is planned in order to identify the optimum SAR sensor configuration and operational mode with reference to the considered application. For urban areas, the SAR simulation tool could be used, for instance, to determine the optimal values of SAR parameters (look angle, radar polarization, altitude, etc.) that maximize the information content in the corresponding SAR images.

Manuscript received September 13, 2002; revised February 17, 2003.

The authors are with the Dipartimento di Ingegneria Elettronica e delle Telecomunicazioni, Università di Napoli "Federico II," 80125 Napoli, Italy (e-mail: daniele.riccio@unina.it).

Digital Object Identifier 10.1109/TGRS.2003.814626

SAR raw signal simulators relevant to natural terrain [3] and ocean [4] scenes have been introduced, validated, and in some cases conveniently applied to actual situations [5], [6]. However, these simulators cannot be applied to man made scene, since the rationales behind scattering and radar models for natural and man-made scenes are completely different.

In this paper, we present the radar and the electromagnetic models that allow to design a SAR simulator able to compute the raw data that would be received by the sensor in an actual mission: the description of the urban scene is required by means of raster data (topography and dielectric constants of the area) and vectorial data (geometry and dielectric constants of the buildings); the description of the SAR sensor is performed through relevant radar and mission parameters. As far as the computation of the raw data is concerned, an analytical model for the SAR transfer function and an analytical electromagnetic model for the scattering from each building in the scene are employed. These analytical models allow to efficiently perform the SAR raw data simulation: the computational time is enormously reduced with respect to any conceivable SAR simulator based on numerical evaluation of the return received in each position of the synthetic antenna; in addition, a SAR simulator would be practically unrealisable without the use of the closed-form analytical electromagnetic models for building backscattering that have been recently introduced by some of the authors [7].

Our analysis begins with the study of the interaction between an the electromagnetic field and a canonical structure which is constituted by a dielectric prism laying on a rough surface, the latter being in principle of infinite extent. When a plane wave impinges on such a structure, single-scattering contributions come back to the sensor, related to the backscattering properties of the ground, the building walls and roof. In addition, part of the electromagnetic wave is double scattered from the ground to the wall and vice versa, and then sent back to the sensor, forming a second contribution to the scattered field. Further contributions are given by triple-scattering phenomena including triple reflections from walls and ground.

It is important to note that in [7] the scattering problem was addressed in the phasor domain, i.e., assuming time harmonic signals; therefore, those results are not straightforwardly applicable whenever a pulsed imaging radar is considered: modifications of results presented in [7] in an appropriate mixed time-phasor domain are here presented (see Section III, which addresses the temporal issues related to the optical path of each electromagnetic wave contribution).

Validity limits of our simulator are essentially related to the applicability of adopted building scattering models. This does not impose significant practical limitations to the SAR simulator since the employed physical optics (PO) and geometrical optics (GO) models widely apply in the high frequency region dictated by the usual operational SAR radar frequencies. Further limitations are the fact that we neglect interactions among different buildings and that the hypothesis of monochromatic wave is adequate as long as the bandwidth is much smaller than the carrier frequency: for resolutions of the order of 1 m, chirp bandwidth is of the order of few hundreds megahertz, so that this can limit the validity of the approach at L-band for very high resolutions (however, C-band and X-band systems can be safely dealt with). Also the assumption of planar facets smaller than resolution but much larger than wavelength may limit the validity of our simulator for very high resolution systems (less than 1 m) at L-band.

The paper is organized as follows. The electromagnetic model and the simulation issues are presented in Section II and in Section III, respectively. Section IV is devoted to present some simulation examples and the rationale for their validation, while in Section V a concluding discussion and ideas for further developments of the simulation tool are proposed.

II. Backscattering Model

Evaluation of multiple scattering from a wall–ground structure is analyzed in great detail in [7]. In this section, we recall results reported in that paper: these results will be inserted in the simulator presented here, as explained in Section III.

The geometrical model consists of a prism whose vertical walls form a generic angle with respect to the sensor line of flight. The prism is placed on a rough surface. The roof and the walls of the building as well as the ground are supposed to be made of lossy dielectric material. Scattering calculations are valid in the "high-frequency" regime, i.e., when dimensions of reflecting objects are much larger than wavelength. The electromagnetic model that we consider is the Kirchhoff approach (KA) in either PO or GO approximations, as better described below. Following this approach, backscattered field is calculated as the sum of elementary contributions from simple objects that form the whole structure. In our case, these elementary scatterers are the building vertical walls and the surrounding ground.

First-order contributions to the radar return are those relevant to each elementary scatterer (terrain, wall, or roof): these contributions have been widely studied in literature and are here referred to as "single-scattering contributions."

Second-order contributions are now analyzed. Our attention is focused on vertical building walls. Part of the incident wave transmitted by the radar is directly backscattered by the vertical walls, but another part is first scattered by the walls toward the ground and then scattered by the ground itself toward the radar. Of course, also the opposite happens: part of the wave scattered from ground directs itself toward the vertical wall and then in the direction of radar. We refer to these mechanisms as "wall–ground reflections" and "ground–wall reflections."

According to the previous rationale third-order contribution can be defined as due to "ground–wall–ground" and "wall–ground–wall" reflections. This latter third-order contribution only arises if the ground is rough: in fact, for 90° dihedral with flat surfaces it is shown that contributions of order greater than two do not arise [8].

In our model, single-scattering contributions are evaluated in the framework of the KA by using either PO or GO depending on surfaces roughness: PO approximation is used for a moderately rough soil, while the GO approximation is used for a very rough soil. In order to account for multiple scattering between buildings and terrain, we use GO to evaluate the field reflected by the smooth wall toward the ground (first bounce) or the sensor (second or third bounce), and GO or PO (depending on ground surface roughness) to evaluate the field scattered by

the ground toward the wall (first or second bounce) or the sensor (second bounce).

Superposition of first-, second-, and third-order contributions fully represent the scattered field; higher order mutual interactions do not give any contribution to the backscattered field to the radar antenna because the wall surface is supposed to be flat.

The rationale for the superposition of the field contributions presented in [7] is here adopted. In particular, note that as second-order contributions we mean the coherent sum of the ground–wall and the wall–ground scattering contributions. In fact, these two contributions run the same optical path and they have to be summed coherently. Conversely, first-, second-, and third-order contributions must be summed up incoherently (i.e., total variance is the sum of their variances), for the reasons explained in [7].

By using the KA, the field scattered by a (possibly rough) surface can be written as [7], [9]

$$\begin{bmatrix} E_{Sh} \\ E_{Sv} \end{bmatrix} = jk\frac{e^{jkr}}{4\pi r}\begin{pmatrix} S_{hh} & S_{vh} \\ S_{hv} & S_{vv} \end{pmatrix}\begin{bmatrix} E_{0h} \\ E_{0v} \end{bmatrix} I_S \tag{1.a}$$

wherein

$$I_S = \int_S e^{j(\underline{k}_i - \underline{k}_s)\cdot\underline{r}'}\, d\underline{r}' \tag{1.b}$$

$$\underline{E}_i = E_0 \hat{e}_i \exp(jk\hat{k}_i \cdot \underline{r}) \tag{2}$$

is the incident field; $\underline{\underline{S}}$ is a matrix accounting for the polarimetric behavior of the scattering surface; k is the wave number; $\underline{r}'$ is the position vector of a surface point; $\underline{r}$ is the position vector of the observation point; and $\hat{k}_i$ and $\hat{k}_s$ are the unit vectors indicating the incidence and scattering direction, respectively. If we assume that the surface height is a random process, integral I_S is a random variable, whose mean and variance are of interest. In particular, under rather wide hypotheses [3], [9], I_S, and hence the scattered field, is a circular Gaussian complex random variable.

The entries of the matrix $\underline{\underline{S}}$, as well as mean and variance of the integral I_S, are evaluated in closed form in [7] for the different single- and multiple-scattering contributions. In particular, expressions for PO single scattering from the wall are reported in [7, Table I] (GO single scattering from wall is null in the backscattering direction); expressions for GO and PO single scattering from terrain are collected in [7, Table II]; GO–GO and GO–PO double scattering are summarized in [7, Tables III and IV], respectively; and finally GO–GO–GO and GO–PO–GO ground–wall–ground triple-scattering contributions are considered in [7, Tables V and VI] (since we use the GO solution for wall scattering, then the ground–wall–ground term does not contribute to the backscattered field).

Expressions reported in [7] have been obtained by assuming that the surface height is a Gaussian random process with Gaussian autocorrelation function. However, extension to the case of a different (e.g., exponential) autocorrelation function can be easily obtained by following the guidelines provided in [7].

Note that in [7] we obtained closed-form solutions, expressed in terms of few parameters. This allows to understand some important characteristics of the scattered field behavior in terms of some of those parameters, and to employ such a model in a simulator. Accordingly, it is possible to easily simulate different scenes only by changing opportune parameters.

III. SAR Raw Signal Evaluation

In this section, we recall the rationale of the SAR raw signal simulation, as implemented in [3]–[6], where only single scattering is considered. Extension to the case of multiple scattering from a wall–ground structure is then presented.

Let us assume that x, r, and ϑ are the coordinates of a ground point in the cylindrical coordinate system whose axis is the sensor line of flight, v is the sensor velocity, and $A_n \equiv (x_n, 0, 0)$ are the antenna positions at times t_n, so that $x_n = vt_n$. At times t_n, the SAR sensor transmits pulses $p(t - t_n)$. Corresponding returns from the considered ground point are attenuated and retarded versions of the transmitted pulses

$$C \cdot p(t - t_n - 2R/c) \tag{3}$$

where $C < 1$ is the attenuation factor; c is the speed of light; and, if single scattering is assumed, then

$$R = \sqrt{r^2 + (x_n - x)^2} \tag{4}$$

is the distance from the sensor to the considered ground point. Accordingly, by letting $r' = c(t - t_n)/2$, moving (for the moment being) to a continuous time formulation, i.e., letting $x' = x_n$, and assuming, as usual, chirp modulation (i.e., linear FM) of the transmitted pulse, we get the following expression for the SAR raw signal (after heterodyne, i.e., downconversion to baseband) [3]

$$\begin{aligned} h(x', r') = \int\int \gamma(x, r) \exp\left[-j\frac{4\pi}{\lambda}\Delta R\right] \\ \times \exp\left[-j\frac{4\pi}{\lambda}\frac{\Delta f/f}{c\tau}(r' - r - \Delta R)^2\right] \\ \cdot w^2\left(\frac{x' - x}{X}\right) \text{rect}\left[\frac{(r' - r - \Delta R)}{c\tau/2}\right] dx\, dr \end{aligned} \tag{5}$$

with $\Delta R = R - r = \sqrt{r^2 + (x' - x)^2} - r$.

In (5), we have the following.

- $\gamma(x, r)$ is the scene reflectivity pattern, proportional to the field backscattered by a small area centered around the point (x, r), divided by this latter area and by the incident field amplitude.
- λ and f are the carrier wavelength and frequency of the transmitted signal, respectively.
- Δf is the chirp bandwidth.
- τ is the pulse duration time.
- $w(\cdot)$ is the azimuth illumination diagram of the real antenna over the ground.
- $X = \lambda R_0/L$ is the real antenna azimuth footprint (we assume that $w(\cdot)$ is negligible when the absolute value of its argument is larger than $1/2$: this assumption could be relaxed at the expenses of time and memory requirements in order to account for the antenna sidelobes).
- L is the azimuth dimension of the real antenna.

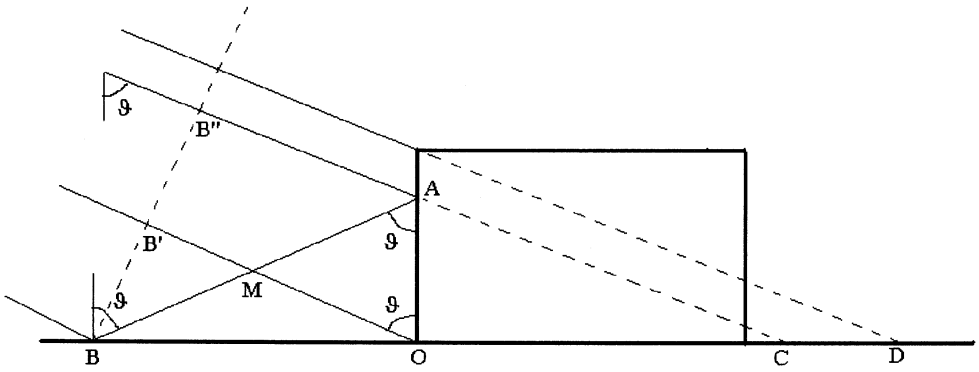

Fig. 1. Optical paths of multiple-scattering contributions.

- rect$[t/T]$ is the standard rectangular window function, i.e., rect$[t/T] = 1$ if $|t| \leq T/2$; otherwise rect$[t/T] = 0$.

According to (5), evaluation of the raw signal can be performed in two steps: in the first one, given the orbit and system data, and assigned the terrain geometric and electromagnetic parameters, the scene reflectivity map is evaluated; in the second step the superposition integral (5) is computed by using an efficient Fourier domain fast Fourier transform (FFT)-based approach. With regard to the first step, the imaged scene surface profile is approximated by rectangular planar facets (smaller than system resolution, but much larger than wavelength), to which a random small-scale roughness is superimposed. The field backscattered by each facet is evaluated as in [3] by taking into account facet slope, roughness and electromagnetic parameters, transmitting and receiving polarizations, and incidence angle, so that the reflectivity map is obtained. PO or GO are used, according to the considered surface roughness. A ground range to slant range projection ensures that foreshortening and layover effects are taken into account [3], whereas a recursive ray tracing procedure identifies the shadowed facets [3]. With regard to the second step, the superposition integral (5) is computed in the Fourier domain by using the asymptotic evaluation of the SAR system transfer function [3] and employing efficient FFT codes. This formulation automatically takes into account range migration effect and variation of focus depth [3]. This described simulator was fully validated by comparison with real SAR images [4]–[6].

Let us now consider how this situation must be modified to include multiple scattering from wall–ground structures (see Fig. 1). In particular, consider a ray that illuminates the scene in the point O and is backscattered, and a double-reflected ray that runs the path A-B and is then scattered toward the sensor. It is not difficult to verify that the path lengths of both rays are equal: in fact, in Fig. 1 we have that $\mathrm{B''A} + \mathrm{AB} = 2\mathrm{B'O}$, because $\mathrm{OM} = \mathrm{AM} = \mathrm{MB}$, so that $\mathrm{AB} = 2\mathrm{OM}$ and $\mathrm{B''A} = 2\mathrm{B'M}$. Hence, the returns corresponding to all of the double-scattered rays share the same time delay, equal to the one of the single-scattering return from the point O. It is important to note that this result is independent of the impact point, the incidence angle and the building height. From this analysis, it is clear that (5) can still be used, provided that a double-scattering contribution is added to the reflectivity map $\gamma(x, r)$ in correspondence of the location of the point $\mathrm{O} \equiv (x, r_{\mathrm{O}})$, i.e., in correspondence of the basis of the wall. Evaluation of the double-scattering contribution is obtained by generating a circular Gaussian complex random variable with mean and variance computed as in Section II.

We now move to consider triple scattering. If we consider triple-scattering ray A−B−A, Fig. 1, it is immediate to see that its optical path is the same of the one of a ray that is backscattered at point C. Hence, the delays of triple-scattering returns are distributed over the interval spanning from the delay corresponding to single scattering from O to the delay corresponding to single scattering from $\mathrm{D} \equiv (x, r_{\mathrm{D}})$. From this analysis, it is clear that (5) can still be used, provided that a triple-scattering contribution is added to the reflectivity map $\gamma(x, r)$, after having evenly distributed it over the range interval from r_{O} to r_{D}. Evaluation of the triple-scattering contribution is obtained by generating a circular Gaussian complex random variable with mean and variance computed as in Section II. This contribution is usually negligible. However, in this case the range allocation is dependent on the incidence angle and on the wall height. Hence, if the acquisition geometry is such that the triple-scattering contribution is in the shadow area, we have that in that area the triple-scattering contribution has to be accounted for and is the dominant one.

As a result of the above considerations, the second step of the simulation procedure [namely, evaluation of (5)] does not need to be changed when considering multiple scattering. Conversely, the first step must be changed as follows. First of all, in addition to orbit, system and terrain data, also building data must be provided as input and stored. In particular, coordinates of vertices of the building projection over the horizontal plane and buildings' heights must be provided. They can be either read from an external file (a dxf file) or provided directly by the user via the computer keyboard. For each facet, the simulation code compares the facet position to the building information, in order to distinguish among the following three cases.

1) The facet is external to all the buildings, i.e., it corresponds to terrain.
2) The facet is within a building, i.e., it corresponds to a building roof.
3) The facet is intersected by one (or possibly more) building external wall.

In the first case, the facet reflectivity is evaluated by using PO or GO single scattering from the rough terrain (see Section II); in

TABLE I
MAIN SAR SENSOR CHARACTERISTICS

Sampling frequency [MHz]	31
Pulse Repetition Frequency [Hz]	350
Look angle [deg]	28
Azimuth antenna dimension [m]	8.5
Range antenna dimension [m]	1.5
Carrier frequency [GHz]	1.28

the second case, PO single scattering from a smooth roof is considered; finally, in the third case first of all the simulation code verifies whether the wall is illuminated: if this is the case, in addition to the usual single scattering, the double-scattering contribution is evaluated and placed at a range position corresponding to the wall basis, and triple-scattering contribution is evaluated and distributed in the proper range interval by using the same "power sharing" technique also employed for the single-scattering case [3].

Iterating the above procedure for all the facets in which the scene is subdivided allows the evaluation of the whole reflectivity map of the scene.

IV. EXAMPLES AND VALIDATION

In order to show some of the potentialities of the simulator in the interpretation of the SAR images, in this section, we present some simulation experiments. The analysis of the obtained results also allows performing a validation of the simulation code.

In the first set of experiments, we have simulated the SAR raw signal from a scene composed of a large building modeled as a parallelepiped with height $h = 40$ m, azimuth dimension 200 m, and with variable range dimension L. In addition, the building has dielectric constant $\varepsilon_r = 3$ and conductivity $\sigma = 0.01$ S/m. The parallelepiped is placed on a rough terrain modeled as a Gaussian process with standard deviation $\sigma = 0.1$ m and correlation length $l = 0.8$ m, with dielectric constant $\varepsilon_g = 4$ and conductivity $\sigma_g = 0.01$ S/m. The line of flight of the sensor, whose main characteristics are presented in Table I, is parallel to a building wall, and the wavelength is 0.234 m. The analysis of such a case allows a validation of the simulator, and it is the milestone for the interpretation of more involved scenarios.

In Figs. 2–4, we show the reflectivity maps relevant to buildings with range dimensions of 200, 60, and 40 m, respectively. Despite of the simplicity of the scene, a visual inspection of the presented images does not allow an easy interpretation of the geometrical and physical characteristics of the building. Hence, a qualitative analysis is here presented in order to understand the formation of the reflectivity map and in order to validate the obtained result.

Since the SAR signal formation is determined by the time arrivals of the pulses to the sensor (see Section III), we set

$$t_i = \frac{2}{c} r_i, \qquad i = 1, \ldots, 5 \tag{6}$$

where r_i are distances between the sensor and scene elements that are located on the equal-range curves depicted in Fig. 5.

Until the time t_1, the sensor receives only the field backscattered from the ground, and the reflectivity function value is determined just by the radar cross section of the rough terrain. In the time interval (t_1, t_2) also, the field backscattered by part of the building roof and by the vertical wall reaches the SAR sensor and enhances the reflectivity function, giving rise to a layover phenomenon. As discussed in the previous section, we expect that all the double-reflection contributions run optical paths of the same length, so they are grouped in the time instant t_2 whatever the illumination angle and the building height are. The discussion of the previous section also allows stating that the SAR sensor receives the triple-reflection contribution in the time interval (t_2, t_3). In addition, it is straightforward to see from Fig. 5 that in the time interval (t_2, t_4) the SAR sensor receives the building roof return, whilst, due to the shadowing phenomenon, no return is detected in the interval (t_4, t_5). From t_5 on, the only contribution to the reflectivity function will be given by the ground scattering.

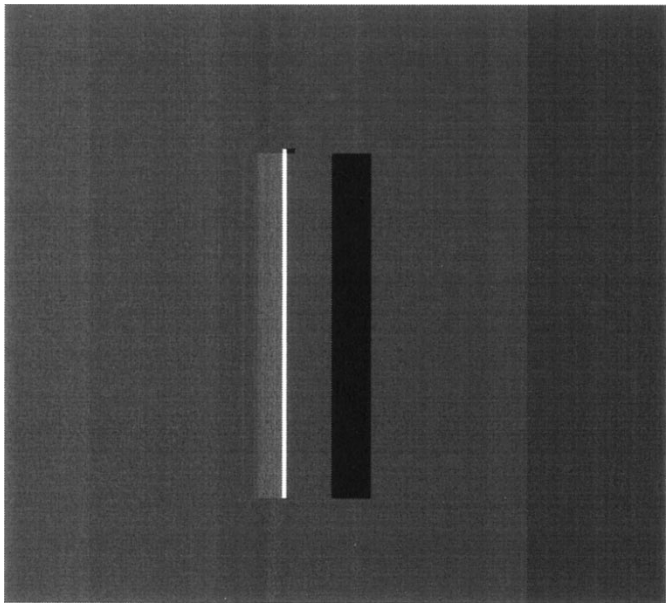

Fig. 2. Reflectivity map relevant to a canonical scene with a large building with height 40 m, azimuth dimension 200 m, and range dimension 200 m. Dielectric constant $\varepsilon_r = 3$ and conductivity $\sigma = 0.01$ S/m. The ground is a rough surface with dielectric constant $\varepsilon_g = 4$ and conductivity $\sigma_g = 0.01$ S/m.

Note that for different building heights or widths or for different look angles, the presented scenario may change, and the reflectivity map (and, as consequence, the SAR images) may assume behaviors considerably different. For instance, if $t_3 < t_4$, all the triple-reflection contribution is received by the sensor together with the field directly backscattered from the building roof; hence, according to what is explained in Section II, it does not appreciably change the radar return. Conversely, if $t_3 > t_4$, the triple-reflection contribution is located in the shadow area, so that it is the only contribution to the SAR signal in that area and cannot be neglected at all. By geometrical considerations, we can state that the condition $t_3 > t_4$ is verified if

$$h > L \sin\theta \cos\theta. \tag{7}$$

Hence, in general, if $h > L/2$ the triple-scattering contribution term always appears in the shadow area whatever the incidence angle is.

In addition, it may occur that $t_4 < t_2$; hence, the whole roof contribution is detected before the double-reflection contri-

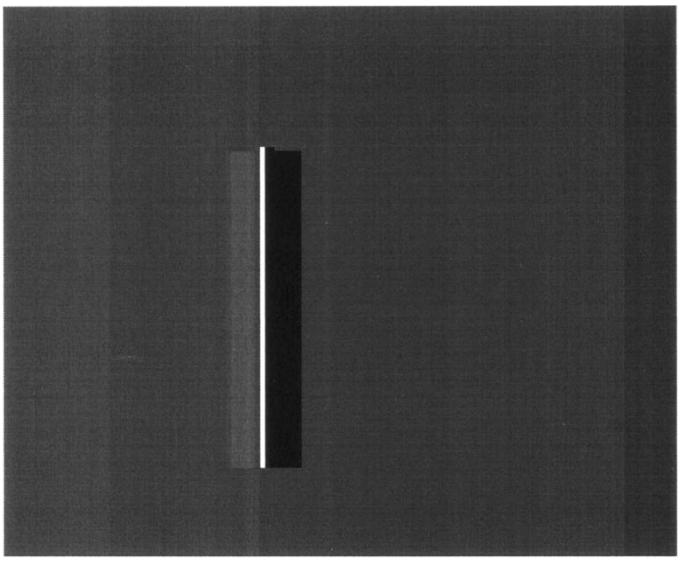

(a)

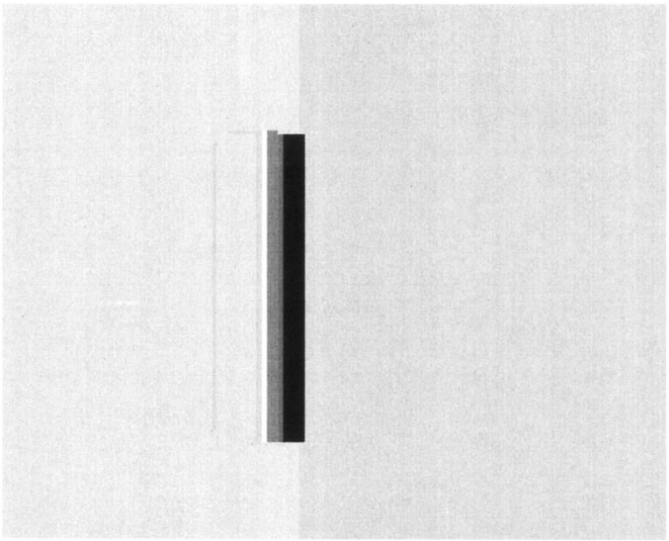

(b)

Fig. 3. (a) Reflectivity map relevant to a canonical scene with building range dimension equal to 60 m. (b) Equalization emphasizes the presence of the triple-scattering contribution. Dielectric constant $\varepsilon_r = 3$ and conductivity $\sigma = 0.01$ S/m. The ground is a rough surface with dielectric constant $\varepsilon_g = 4$ and conductivity $\sigma_g = 0.01$ S/m.

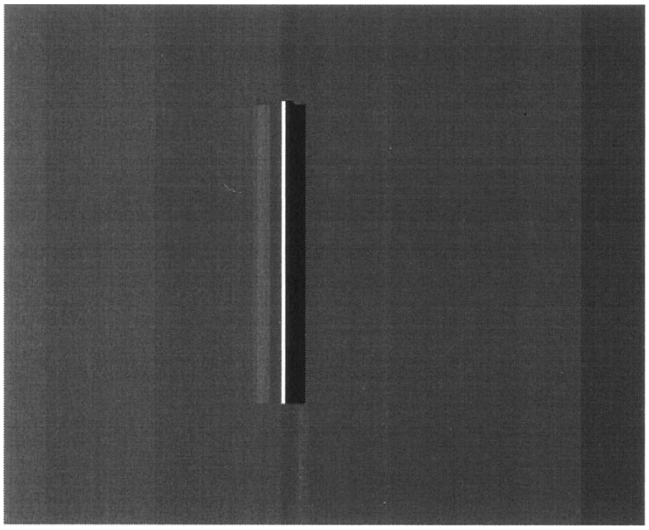

(a)

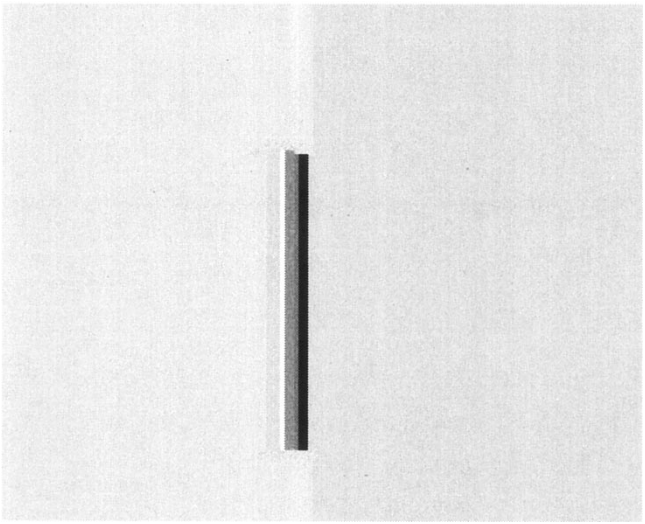

(b)

Fig. 4. (a) Reflectivity map relevant to a canonical scene with building range dimension equal to 40 m. (b) Equalization emphasizes the presence of the triple-scattering contribution. Dielectric constant $\varepsilon_r = 3$ and conductivity $\sigma = 0.01$ S/m. The ground is a rough surface with dielectric constant $\varepsilon_g = 4$ and conductivity $\sigma_g = 0.01$ S/m.

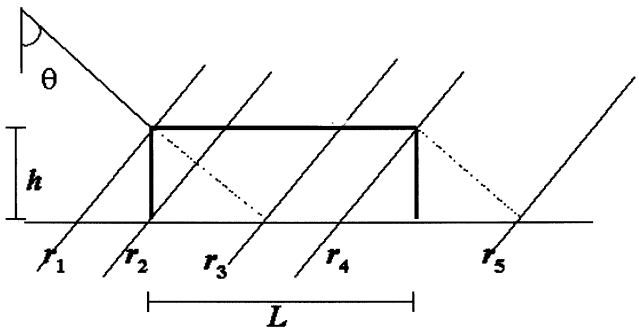

Fig. 5. Geometry of the radar acquisition.

bution. The high number of possible scenarios emphasizes the value of a simulator able to reproduce automatically different cases and to understand the physics.

By looking now at Fig. 2 from left to right, we can recognize the layover area, then the brightest double-reflection line, the building roof contribution, and the shadow. The electromagnetic returns are in the order described by Fig. 5, according to the high value of the building range dimension L. Triple-reflection contribution is completely hidden by the stronger roof backscattering contribution, according to (7).

By reducing the range dimension to 60 m in order to fulfil condition (6), we get the reflectivity map of Fig. 3, whose inspection suggests some considerations. In particular, by analyzing Fig. 3(a) from left to right, we still easily recognize the layover and the double-reflection effects as bright areas; in addition, we see a darker area between the layover and the double reflection. Such an effect is due to the fact that the reduction of the building dimension led to the condition $r_4 < r_2$; hence,

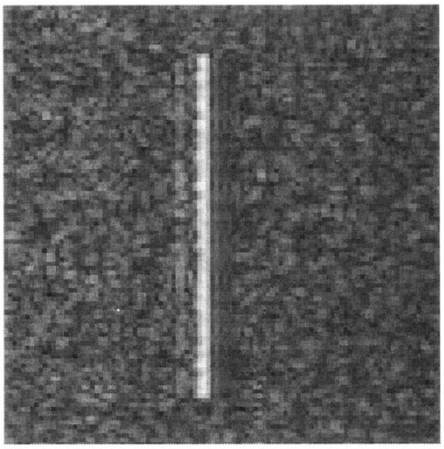

Fig. 6. Simulated single-look SAR image relevant to a canonical scene with building range dimension equal to 60 m. Dielectric constant $\varepsilon_r = 3$ and conductivity $\sigma = 0.01$ S/m. The ground is a rough surface with dielectric constant $\varepsilon_g = 4$ and conductivity $\sigma_g = 0.01$ S/m.

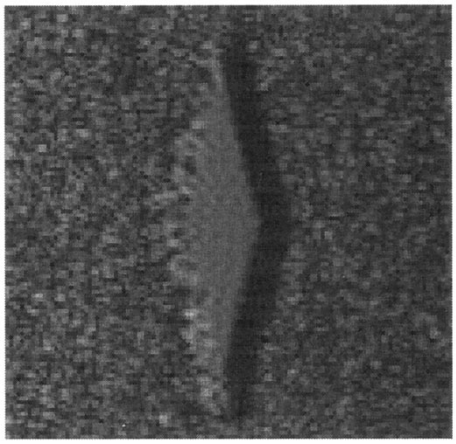

Fig. 7. Simulated single-look SAR image relevant to a canonical scene with building range dimension equal to 60 m. Dielectric constant $\varepsilon_r = 3$ and conductivity $\sigma = 0.01$ S/m. The angle between SAR line of flight and the building wall is 45°. The ground is a rough surface with dielectric constant $\varepsilon_g = 4$ and conductivity $\sigma_g = 0.01$ S/m.

the whole roof contribution is located before the double reflection, and the darker area is a region where only the terrain and the wall contribution are present. Inspection of Fig. 3(a) does not allow the identification of the triple-reflection contribution; hence, we performed an equalization that saturates the highest and enhances the lowest values, so that in Fig. 3(b) we can recognize the triple-reflection contribution in the shadow region.

In order to further emphasize the introduced concepts, we have reduced the building range dimension to 40 m, so that in Fig. 4, we can easily separate the different contributions. The obtained image is in agreement with presented theoretical consideration.

The reflectivity map presented in Fig. 3 has been processed by the SAR raw signal simulator, according with the rationale presented in Section III. The obtained result has been employed as input in a standard SAR processor, in order to generate the corresponding SAR image, presented in Fig. 6. Azimuth and range pixel dimensions of the image are 2.57 and 4.83 m, respectively.

In the following, we consider that the SAR sensor line of flight is not parallel to one of the building walls. In particular, we consider that the angle between the vector line of flight and the wall orientation is 45°. In Fig. 7, we present the obtained SAR image, where we recognize that at 45° the double-reflection contribution is not dominant, as predicted by the theory (see Section II and [7]).

Introduced considerations give us now the chance to analyze more complex situations, by changing the scene or the sensor parameters. Dependences on the look angle, frequency, height of flight of the sensor, dielectric constant, shape, dimension of the building, terrain roughness and dielectric properties, and so on can be explored. The simulation of different scenes can also allow the realization of databases useful for inversion purposes.

As an example, we can compare the SAR images relevant to buildings of different materials. In particular, in Fig. 8 the SAR image is relevant to a scene composed of two buildings: the one located in the lower half of the figure has a dielectric constant $\varepsilon_r = 4$ (typical of dry concrete) and the one located in the upper half of the figure of dielectric constant $\varepsilon_r = 7,5$ (typical of limestone). The difference between the dielectric constants causes a slight difference in the single scattering; hence, it does not allow an easy classification by means only of the roof return. But in the double-reflection return, the signals are integrated over an area whose dimension depends on the building height, so the difference between the returns is magnified. The effect of the sidelobes of the double-scattering return over the upper building is also apparent in this figure.

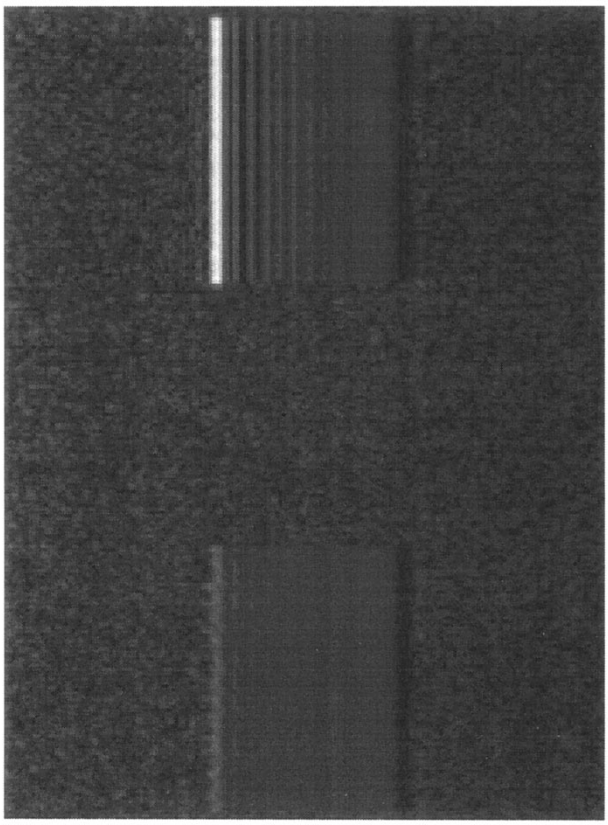

Fig. 8. Simulated single-look SAR image of a scene with two buildings, both of 400×400 m^2, with dielectric constant $\varepsilon_r = 4$ and $\varepsilon_r = 7,5$ and conductivity $\sigma = 0.01$ S/m and $\sigma = 0.03$ S/m, respectively. The ground is a rough surface with dielectric constant $\varepsilon_g = 4$ and conductivity $\sigma_g = 0.01$ S/m.

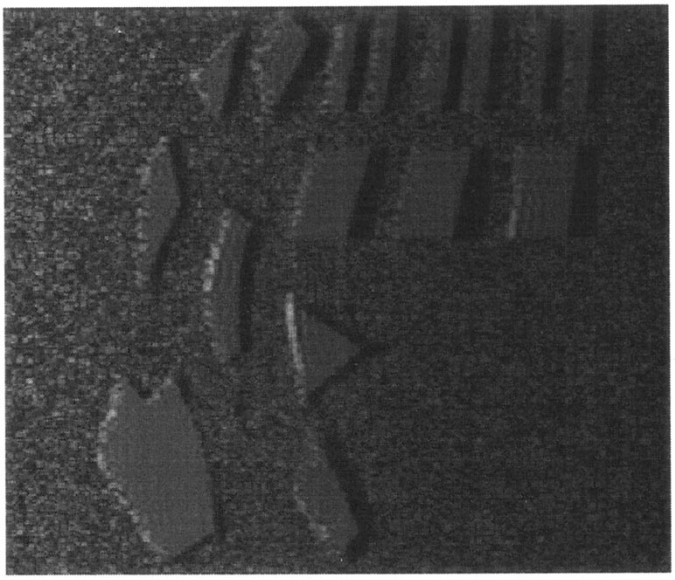

Fig. 9. Simulated single-look SAR image of a scene with 16 buildings with different dielectric constants and conductivities. The ground height profile is a Gaussian hill. Its maximum height is 150 m. The ground is a rough surface with dielectric constant $\varepsilon_g = 4$ and conductivity $\sigma_g = 0.01$ S/m.

Urban settlements are more complex environments than the presented canonical cases; hence, we have simulated a more involved scene with 16 buildings with different characteristics. In addition, the ground is not flat, but it is a hill described by means of a Gaussian height function. In Fig. 9, we show the obtained simulated image, whose inspection suggests some consideration. In particular, we can see that the simulator runs with buildings of any shape; we can recognize how the layover, shadowing, and multiple-reflection contributions change for different scenarios.

In addition, SAR simulation can suggest new hints for several fields of applications. For instance, in the upper part of the simulated image, we can appreciate a more regular urban structure, while in the rest of the scene the shape and location of buildings is more irregular, emphasizing possibilities of SAR in solving problems of city classification.

In conclusion, we discuss the computational time required to realize the presented simulations. Note that a conventional SAR processing has to be applied to get the SAR images from the corresponding SAR simulated raw signals: hence, the study is here only focused on the computational time for obtaining the SAR raw signal from the scene input data and the SAR mission parameters. We have employed a Pentium IV personal computer with a 1.7-GHz processor. The dependence of the computational time on the scene characteristics has been studied. In particular, as far as the images presented in Figs. 2–4 and 6 and 7 are concerned, they are images of 512 × 512 pixels with a single building. The computational time for the corresponding raw signal has been almost the same for all the mentioned scenes, and its value is about 34 s. Then, several raw data have been generated, by changing the building dimension and the number of building walls: the corresponding computational times turned out to be constant within a margin of 3%. Conversely, the computational time is clearly affected by the number

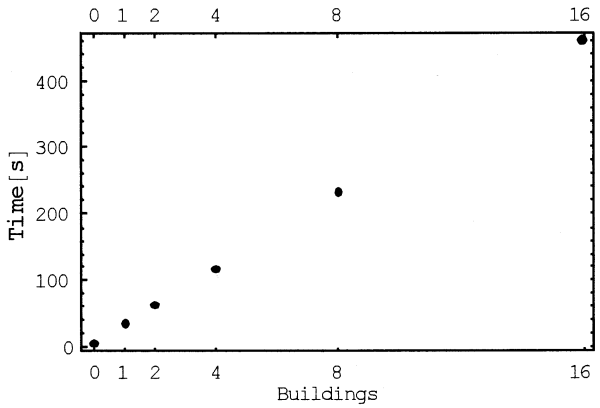

Fig. 10. Computational time as a function of the number of buildings in a scene of 512 × 512 pixels.

of buildings in the scene; by increasing the number of buildings, the computational time increases in an almost linear way. This result can be somehow forecasted by inspecting the theoretical models we adopted: in fact, the presented urban structure simulator holds different and very complicated scattering models with respect to any other efficient terrain simulator [3], [5]; as a matter of fact, the simulation time is mainly devoted to project the building elements in the azimuth–slant range coordinates, determine the areas interested in the multiple-scattering events, and evaluate the scattering coefficients for those elements. Hence, in this urban structure simulator, the evaluation time of procedures that are in common with previous simulators [3], [5] turn out to be almost negligible. In Fig. 10, the computational time in seconds as a function of the number of buildings is shown. Such a graph provides also the time employed to generate images of Figs. 8 and 9, i.e., $1'02''$ and $7'38''$, respectively.

V. Conclusion, Further Developments, and New Perspectives

A SAR raw signal simulator for urban scenes has been presented. A full discussion to emphasise main novelties and differences with respect to other existing simulators only applicable to natural scenes has been provided.

The proposed simulator relies on a backscattering and an imaging radar model. Urban areas are represented as dielectric buildings over a random rough nonflat dielectric terrain. The adopted scattering model holds under the Kirchhoff approximation and takes into account any order (single and multiple) scattering contribution forecasted by the adopted geometrical model of the scene. In the presented electromagnetic model, any scattering contribution is evaluated in closed form so that a reasonable and feasible numerical computations is simply required: in fact, the backscattering coefficients evaluation only implies computing some algebraic parametric formulas instead of numerically solving integrals or integral equations. The adopted radar model efficiently operates in the two-dimensional Fourier-transformed domain. It turns out that the presented SAR raw signal simulator is feasible in terms of computational time.

Simulated SAR images are easily obtained from the corresponding simulated SAR raw signals by means of a standard

SAR processor. Reported examples show that the presence of buildings over the simulated SAR images produces effects that are qualitatively consistent with what was expected from theoretical considerations. In addition, it is here stressed that the simulated images provide also a fundamental quantitative assessment to those qualitative considerations.

Moreover, reported examples suggest two possible applications of the proposed simulation tool. On one side, our simulator is able, for a fixed urban scene, to quantitatively assess the effect on achievable SAR images whenever the SAR sensor parameters (altitude and direction of flight, look angle, polarization, radar frequency and bandwidth, sampling frequency along azimuth and range, antenna patterns, etc.) are changed. On the other side, our simulator is able, for a fixed SAR sensor configuration, to quantitatively assess the effect on SAR images of parameters relevant to buildings (dimensions, position, and orientation over the scene, complex dielectric constants) and/or the surrounding terrain (morphology, complex dielectric constants). The proposed simulator turns out to be also eligible for training numerical schemes devoted to feature extraction (e.g., neural networks) and to test any specific SAR processing or postprocessing technique.

A comment on the complexity of the model used to describe the buildings in the urban area is now in order. It may appear that the adopted geometrical model for the buildings is rather simplified. The answer to this observation is twofold. First of all, the building input data required in the proposed version of the simulator are usually the only achievable ones in a field campaign performed by means of aerophotogrammetry or by digitalizing data from urban databases. Second, even in the case that more detailed data concerning the building shapes (e.g., building description including appropriately spaced balcony and/or windows along the vertical direction, and different materials along the horizontal direction) are available, the presented simulator can be appropriately extended considering the proposed backscattering and radar models. In fact, as far as the horizontal direction is concerned, a more complete description for the buildings can be included in the input dataset without changing the scattering and radar models employed in the simulator. As far as the vertical direction is considered, it is conceivable to appropriately reapply, to balcony and window structures, the same rationale used to evaluate the radar single- and multiple-scattering contributions from wall–ground structures, and then positioning these contributions onto the reflectivity map as a function of the two-way ray path from the sensor line of flight to the building; in this case, power-sharing and GO-based approaches can be considered to determine the amount of the incident power over each portion of the building. These further developments of our simulator will be certainly explored as soon as such a detailed field campaign on buildings shape is available.

REFERENCES

[1] F. M. Henderson and Z. Xia, "SAR applications in human settlement detection, population estimation and urban land use pattern analysis: A status report," *IEEE Trans. Geosci. Remote Sensing*, vol. 35, pp. 79–85, Jan. 1997.

[2] Z. Xia and F. M. Henderson, "Understanding the relationships between radar response patterns and the bio- and geophysical parameters of urban areas," *IEEE Trans. Geosci. Remote Sensing*, vol. 35, pp. 93–101, Jan. 1997.

[3] G. Franceschetti, M. Migliaccio, D. Riccio, and G. Schirinzi, "SARAS: A SAR raw signal simulator," *IEEE Trans. Geosci. Remote Sensing*, vol. 30, pp. 110–123, Jan. 1992.

[4] G. Franceschetti, M. Migliaccio, and D. Riccio, "On ocean SAR raw signal simulation," *IEEE Trans. Geosci. Remote Sensing*, vol. 36, pp. 84–100, Jan. 1998.

[5] ——, "SAR raw signal simulation of actual scenes described in terms of sparse input data," *IEEE Trans. Geosci. Remote Sensing*, vol. 32, pp. 1160–1169, Nov. 1994.

[6] G. Franceschetti, A. Iodice, D. Riccio, G. Ruello, and R. Siviero, "SAR raw signal simulation of oil slicks in ocean environments," *IEEE Trans. Geosci. Remote Sensing*, vol. 40, pp. 1935–1949, Sept. 2002.

[7] G. Franceschetti, A. Iodice, and D. Riccio, "A canonical problem in electromagnetic backscattering from buildings," *IEEE Trans. Geosci. Remote Sensing*, vol. 40, pp. 1787–1801, Aug. 2002.

[8] T. Griesser and C. A. Balanis, "Backscatter analysis of dihedral corner reflectors using physical optics and the physical theory of diffraction," *IEEE Trans. Antennas Propagat.*, vol. 35, no. 10, pp. 1137–1147, 1987.

[9] L. Tsang, J. A. Kong, and R. T. Shin, *Theory of Microwave Remote Sensing*. New York, NY: Wiley, 1985.

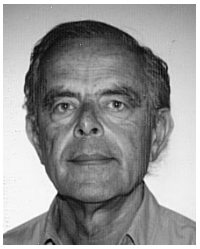

Giorgio Franceschetti (S'60–M'62–SM'85–F'88–LF'01) was born in Italy.

He is currently a Full Professor of electromagnetic wave theory at University of Naples, Naples, Italy, since 1968. He is also an Adjunct Professor at the University of California, Los Angeles (UCLA) and a Distinguished Visiting Scientist at the Jet Propulsion Laboratory, California Institute of Technology (Caltech), Pasadena. He was a Visiting Professor at the University of Illinois, Urbana-Champaign, in 1976 and 1977, and at the UCLA in 1980 and 1982. He was a Research Associate at Caltech, in 1981 and 1983, a Visiting Professor at National Somalia University, Mogadishu, Somalia, in 1984, and a Visiting Professor at the University of Santiago de Compostela, Santiago de Compostela, Spain, in 1995. He has published several books and more than 130 refereed papers in the field of applied electromagnetics (reflector antennas, transient phenomena, shielding, nonlinear propagation, and scattering) and, more recently, in the field of SAR data processing and simulation. He has lectured in several summer schools in China, the United Kingdom, Holland, Italy, Spain, Sweden, and the United States.

Dr. Franceschetti was a Fulbright Scholar at Caltech in 1973. He has been the recipient of several national and international awards. He was Director of IRECE, a Research Institute of the Italian National Council of Research (CNR), and member of the board of the Italian Space Agency (ASI).

Antonio Iodice (S'97–M'00) was born in Naples, Italy, on July 4, 1968. He received the laurea degree (with honors) in electronic engineering and the Ph.D. degree in electronic engineering and computer science from the Univeristy of Naples, Italy, in 1993 and 1999, respectively.

In 1995, he received a grant from CNR (Italian National Council of Research) to be spent at IRECE (Instituto di Ricerca per 1'Elettromagnetismo e i Componenti Elettronici), Naples, for research in the field of remote sensing. He was with the Department of Electronic and Telecommunication Engineering, University of Naples, from 1996 to 1999, and with Telespazio S.p.A., Rome, Italy, from 1999 to 2000. He is currently a Research Scientist at the Department of Electronic and Telecommunication Engineering, University of Naples. His main research interests are in the field SAR remote sensing, modeling of electromagnetic scattering from natural surfaces, and SAR interferometry.

Daniele Riccio (M'91–SM'99) was born in Naples, Italy, on April 13, 1962. He received the laurea degree (with honors) in electronic engineering from the University of Naples "Federico II," Naples, Italy, in 1989.

Currently, he is Professor of remote sensing, electromagnetic diagnostics, and guided propagation at the University of Naples "Federico II." He was a Research Scientist at the Istituto di Ricerca sull'Elettromagnetismo e i Componenti Elettronici (IRECE), Italian National Council of Research (CNR), and at the Department of Electronic and Telecommunication Engineering, University of Naples "Federico II." In 1994 and 1995, he was also a Guest Scientist at the DLR High-Frequency Institute, Munich, Germany. His main research activities are in the fields of microwave remote sensing and simulation and modeling of SAR signals relevant to terrestrial and oceanic scenes, as well as in the application of fractal geometry to electromagnetic scattering and remote sensing.

Prof. Riccio has won several fellowships from private and public companies (SIP, Selenia, CNR, CORISTA, and CRATI) for research in the remote sensing field.

Giuseppe Ruello (S'00) was born in Naples, Italy, on February 12, 1975. He received the laurea degree (with honors) in telecommunication engineering, in 1999, and the Ph.D. degree in electronic and telecommunication engineering, in 2003, both from the University of Naples "Federico II," Naples, Italy.

In 2000, he received a grant from the University of Naples to be spent at the Department of Electronic and Telecommunication Engineering for research in the field of remote sensing. In 2000, he won also a grant from the University of Rome "La Sapienza," Rome, Italy. In 2002, he was a Visiting Scientist at the Department of Signal Theory and Communications of the Universitat Politecnica de Catalunya, Barcelona, Spain. His main research interests are in the field of SAR remote sensing, modeling of electromagnetic scattering from natural surfaces, and SAR simulation.